University of Glasgow

DEPARTMENT OF

AEROSPACE ENGINEERING

An examination of the dynamic stalling of two wing planforms

by

S. Moir and F.N. Coton

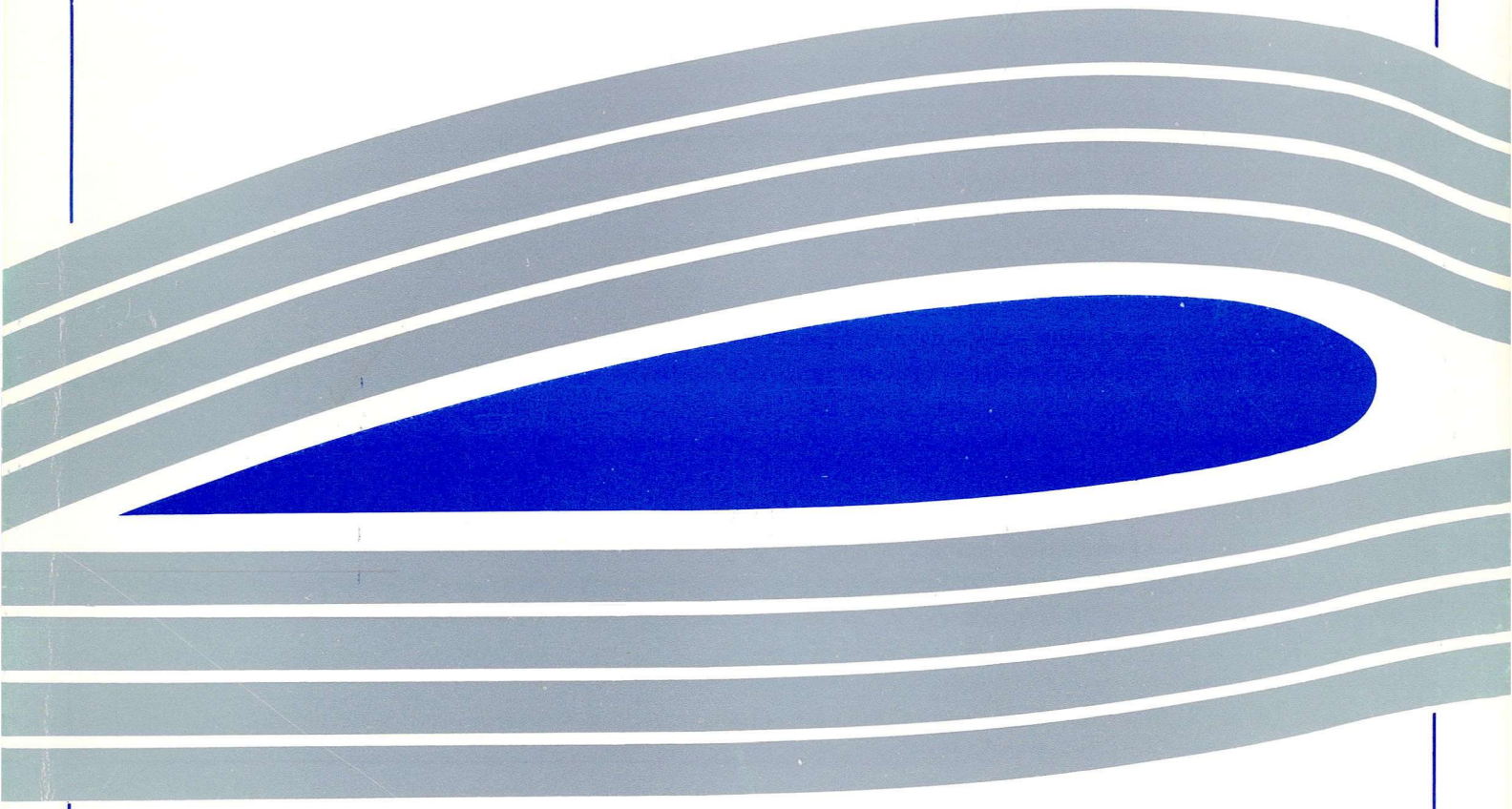

An examination of the dynamic stalling of two wing planforms

by

S. Moir and F.N. Coton

December 1995

G.U. Aero. Report 9526

An examination of the dynamic stalling of two wing planforms

by

S. Moir & F.N. Coton
Department of Aerospace Engineering
University of Glasgow
Glasgow G12 8QQ

INTRODUCTION

Almost all dynamic stall experiments to date have considered the nominally two-dimensional case. These investigations have contributed to an improved understanding of fundamental phenomena associated with helicopter rotor blades and, as a result, the shape of these blades has steadily evolved. A key element of this technology, however, is the design of the blade tip which is exemplified by the BERP design with its large swept tip and the notch at the blade/tip junction. These features are in regions where the air flow over the blade is strongly three-dimensional and, consequently, data sets obtained from two-dimensional experiments are not representative and can provide no insight as to the dominant flow mechanisms there. Whilst it is known that the tip shape has a significant effect on the stalling process of the blade, the current inability of aerodynamic modelling procedures to quantify this effect limits further development and refinement of tip shapes.

In the absence of a detailed theoretical model, evolution of the blade-tip planform has been achieved by the application of a combination of fixed wing aerodynamic principles, test results and logical deductions. The aerodynamic models that are available for rotor aeroelastic calculations are extremely limited and, generally, require sweeping assumptions to be made: particularly in the area of flow separation and stall which is critical to the helicopter design process. In the long term, computational fluid dynamics may offer solutions to the flow problem but, given current limitations, cannot realistically be expected to provide one of the inner loops of an overall aeroelastic response calculation for the foreseeable future. In the meantime, there is a pressing need for an analysis technique containing enough detail to allow refinements of helicopter rotor tip planform design.

Development of this kind of model and further extension to deal with external vortex loading effects under dynamic conditions is currently hindered by a lack of physical data . Thus, to provide a comprehensive model, it is necessary to obtain information on vortex loading effects, kink effects at centre section and tips and the effects of sweep on the separation process. Wind tunnel testing of finite wings in unsteady conditions can provide this information by exposing the individual effects that require modelling.

To date, very few experiments have been conducted to assess three-dimensional flow effects. Most of these have been reviewed by Carr [1], although the recent studies of Peziali[2] and Horner et al. [3] in this area are particularly noteworthy.

A study is presently underway at Glasgow University to examine three-dimensional dynamic stall by measuring unsteady pressure distributions on three different wing planforms[4]. The work described in this report involved utilising flow visualisation to provide additional information on the structure and behaviour of the unsteady flow field for two finite wing planforms; a straight rectangular wing and a rectangular wing with swept tips which were geometrically similar to those used in the pressure measurements tests. The study concentrated on the specific effects of tip geometry on the off-body flow structures which cannot be fully identified by surface pressure measurements alone. In particular, the evolution of the dynamic

stall vortex and its interaction with the tip vortices, was examined in detail. Many of the features identified in the study were found to be common to the two planforms although the extent of the interaction between the two main vortex structures was substantially different in the two cases. The downstream convection of the dynamic stall vortex was found to be particularly sensitive to this effect.

METHODS

Tests were conducted in the University of Glasgow 0.91m x 0.91m flow visualisation wind tunnel. The pitching motion of the model was generated by use of a stepper motor/lead screw system. The stepper motor was programmed using LABVIEW running on a Macintosh LCIII computer with a data acquisition board installed. Smoke was produced by vaporising Ondina oil in a Taylor Scientific smoke generator and was introduced to the flow either through small holes in the model surface or from a smoke-rake positioned upstream of the model. The general test set-up is shown in Fig. 1.

Images were recorded using a camcorder and then transferred to digital form via a Macintosh based frame grabbing system. Finally, individual frames presented in this report were exported to image processing software, where brightness and contrast were modified to enhance the images.

The two models used in this study were a rectangular wing of aspect ration 3.0 and a rectangular wing with the same chord and trailing edge length but with 60° swept tips. The overall dimensions of the rectangular wing were 200mm x 600mm. Both models were made from wood and had a NACA 0015 cross-sectional profile. The rectangular wing was inlaid with a series of tubes to allow ducting of smoke to lines of holes on the model surface. These holes were located along the leading and trailing edges and on chordal lines at six spanwise positions. By varying the connection of the smoke supply tube to the model, it was possible to select the region of the surface to which smoke was introduced. The swept tip model did not have this facility.

Each model was pitched about its quarter chord line from 0 to 40° at a reduced pitch rate of approximately 0.08. The model was then held at 40° until the main dynamic features of the flow had developed and convected from the trailing edge. The incidence profile against time is shown in Fig. 2. All tests were conducted at a Reynolds number of approximately 13,000.

RESULTS

Rectangular planform

In this section, a number of images are presented which highlight the dominant features of the unsteady flow field around a pitching rectangular wing of NACA 0015 cross-section. In this particular case, the wing is pitched from 0 to 40°, at a reduced pitch rate of 0.08, and then held stationary to allow the continued development of the flow. To provide a comprehensive description of the inherent three-dimensionality of the flow, it was necessary to obtain images from several different viewing angles. Correlation between these different views, was obtained by recording the elapsed time between the start of the pitching motion and the capture of a particular frame. Each image is, therefore, annotated with this information.

In Fig. 3., a series of cross-sectional images of the flow field at the 57% of span location are presented. Initially, the flow behaves in accordance with conventional understanding of 2-D aerofoil behaviour at low Reynolds numbers, with trailing edge separation apparent at very low angles of attack. As the incidence increases, however, the pitch rate appears to suppress the forward movement of the separation point such that, at t=0.52 (α=26°) separation has apparently only progressed to around 60% of chord. What is less visible in this image is that a thin layer of reversed flow has developed over most of the upper surface and is terminated at a

small disturbance near the leading edge. This disturbance grows quite rapidly and by t=0.76 (a = 38°), has formed into a coherent vortex structure which is recognisable as a classical dynamic stall vortex. It is also interesting to note, at this stage, that the fluid within the separation zone is amalgamating into a secondary vortex system which is often referred to as a shear layer vortex. The flow field continues to develop even when the wing has stopped pitching and by t=0.92 the dynamic stall vortex has increased its size and moved slightly rearwards.

By t=1.0 the dynamic stall vortex has moved further towards the trailing edge and into closer proximity with the shear layer vortex. Clearly, the dynamic stall vortex is the more dominant system and, at t=1.12, it is observed to absorb the smaller vortex. In this frame, it is also evident that the dynamic stall vortex has lifted from the wing surface and, as the images at t=1.2 and t=1.36 illustrate, this progression continues until the vortex leaves the domain of the wing at around t=1.76.

A similar series of images, corresponding to the 73% of span location, are presented in Fig. 4. Here the same basic features as those observed further inboard are present in the first two images. Once again, at t=0.92 the general appearance of the flow is similar to its counterpart at 57% of span. What is not immediately obvious in this frame is a slight out of plane rotation of the vortex system. This becomes more apparent at t=1.0 as the vortex moves closer to the shear layer vortex which, itself, has little coherence. The continued rotation of the dynamic stall vortex is quite clear by t=1.12 where the vortex is tornado-like in appearance but is still, apparently, tethered to its point of origin. Nevertheless, there is a clear rearwards progression of the main body of the vortex system and, by t=1.36, it has almost reached the trailing edge. Interestingly, it also appears to have moved closer to the wing surface in this frame. Thereafter the vortex convects towards the trailing edge, dissipating until it can no longer be identified at t=1.84.

Further outboard, at 90% of span, it may be anticipated that three-dimensional effects would be much more significant. These effects make the collection of images akin to those presented above more difficult as much of the flow is out of the viewing plane. Nevertheless, images have been obtained (Fig. 5.) which show that the initial formation of a dynamic stall vortex and disturbances in the shear layer are discernible at t=0.72. The dynamic stall vortex quickly loses definition as a strong spanwise motion inboard predominates over the first 30% of chord. The flow, however, remains highly arched over the front portion of the chord and there is some evidence of a shear layer vortex near the trailing edge. As the flow develops, this shear layer vortex becomes less distinct and is replaced by an increasingly stronger tip vortex.

A different perspective of the flow development is shown in Fig. 6 where the wing is viewed from above and behind and smoke is supplied through the leading edges and tips of the wing. At t=0.64, the dynamic stall vortex is visible as a disturbance in the smoke lines at approximately the quarter chord position. It appears to be less well-defined in the region of the tip vortex but, at this stage, the flow field is still predominantly two-dimensional. The images recorded at t=0.96 and t=1.04 are consistent with those taken from the side which indicated that subsequent development of the dynamic stall vortex was dependent on spanwise location. In the mid-span region, the vortex grows and convects two-dimensionally until it reaches mid-chord. Further outboard, growth and convection are inhibited and, at the very tips, the vortex appears to remain attached to the leading edge. Simultaneously, the smoke in the shear layer begins to coalesce until it forms a thick white band across the entire span close to the trailing edge. With reference to the side views presented earlier, this amalgamation of smoke most likely corresponds to the strengthening of the shear layer vortex. At t=1.04, this band of smoke becomes subtly distorted indicating that the shear layer is now interacting with the dynamic stall vortex whilst maintaining some connection with the tip vortex.

The sequence of events that follow appear to involve complex vortical interactions in what can be described as a strongly three-dimensional flow field. There is apparently no further chordwise convection of the dynamic stall vortex at this stage but, from the information presented in the side views, the section of the vortex at the mid span is lifting away from the surface whilst continually drawing in the shear layer. The displacement of the shear layer can be

seen in the frames corresponding to t=1.04 and t=1.36 as the thick band of smoke becomes significantly altered near the mid-span.

At t=1.36 the change in orientation of outboard sections of the dynamic stall vortex, to accommodate the lifting of the mid-span segment, becomes more apparent. The most significant changes occur at around 73% of span where the side view pictures indicated that the axis of rotation of the vortex became almost normal to the wing surface between t=0.92 and t=1.28. It was also noted that these sections of the vortex appeared to be slightly elevated from the surface as they changed their orientation but moved closer to the wing surface again at approximately t=1.36. In Fig.6, this coincides with the appearance of two counter-rotating swirls of smoke in the region of 73% of span which become more clearly defined with increasing time. By t=1.52, the swirls are noticeably stronger but still appear to retain connectivity with the leading edges of the wing tips through the furthest outboard sections of the dynamic stall vortex. There is also a band of smoke close to the trailing edge which appears to link the counter-rotating vortices to the trailing edges of the wing tips.

Figure 7 presents a final series of views, taken from in front of the wing, which provide further evidence of the behaviour and connectivity of the flow structures identified above. In particular, the mid-span buckling of the dynamic stall vortex is clearly evident at t=1.04 and t=1.2. Furthermore, these pictures suggest that the dynamic stall vortex is still a continuous flow structure, maintaining spanwise connectivity with the less well-developed outboard sections. This is still the case as the central portion of the vortex continues to lift (t=1.36) forming an arch-like structure with the counter-rotating segments identified in other views. The area of smoke in the centre below this arch is evidence of the shear layer being drawn into the dynamic stall vortex. Another interesting feature depicted in this image is the apparent amalgamation of the, previously distinct and well-defined, tip vortex and the main body of smoke.

From t=1.56 onwards, the smoke at mid-span becomes increasingly diffuse whereas, in the region of the tip vortex, it becomes more dense and covers a larger area of the wing. Despite this, the counter-rotating segments are still in evidence but appear to become more inclined to the direction of flow. By t=2.08, no discernible flow structures, are evident on inboard sections of the wing.

Swept-tip planform

In this section, results of flow visualisation tests on a rectangular wing with swept tips are presented for the same test conditions as the rectangular wing in the previous section. Unlike the previous case, however, it was not possible to introduce smoke through the wing surface and so all tests involved the introduction of smoke lines upstream of the model.

Figure 8 shows the development of the flow at the 52% of span position compared to the equivalent images from the rectangular wing tests. As may be observed, the flow characteristics in the first two frames are very similar to those of the rectangular wing with the dynamic stall vortex forming close to the leading edge and an agglomeration of shear layer vorticity towards the trailing edge. The first significant difference between the two can be seen at t=0.96, where the core of the dynamic stall vortex over the swept wing appears to be elevated from the surface. This vortex also seems to be weaker than its more dominant straight wing counterpart. It continues to lift from the wing between t=1.04 and t=1.2 but, unlike the rectangular wing case, shows no signs of interacting with the shear layer vortex. In fact, at t=1.2 the core of the dynamic stall vortex is very high above the wing and the shear layer vortex is just about to convect off the trailing edge. After this, the dynamic stall vortex moves slightly rearwards until t=1.28 when it appears to stop and be held in position above the wing Also at t=1.28, a small cohesive secondary vortex which has been shed from the leading edge region is discernible. In the next two frames, this vortex amalgamates with the dynamic stall vortex which appears to dissipate considerably. Corresponding frames for the straight wing demonstrate the steady progression of the dynamic stall vortex as it convects further downstream, away from the surface. At t=1.52, the dynamic stall vortex above the swept wing appears to be pulled down

towards the surface slightly. Thereafter, it breaks up over the wing and the flow reverts to the bluff-body state.

Further outboard at 57% of span (Fig. 9), initial development of the dynamic stall vortex is once again almost two-dimensional with the same basic features apparent as those present on the straight wing. Very quickly, however, it becomes obvious that further development of the vortex structure is suppressed with a weaker, more elongated vortex evident at t=0.96. Despite this, the shear layer vortex is still clearly visible. It is also relevant to note that the poor definition of the dynamic stall vortex in this image is partially due to a strong inboard spanwise flow, over the first 50% of chord, which draws the smoke out of the viewing plane. As the flow develops further, the vortex becomes even less distinct and the smoke over the front portion of the aerofoil lifts away from the surface. By t=1.16, this area of smoke is established as a vortex which is elevated from the surface and rotating about an axis perpendicular to the chordline. This appears to be similar to the tornado-like vortex structure which was observed above the straight wing at 73% of span. Also visible in this image is the apparent convection of the shear layer vortex from the trailing edge. This is in contrast to the straight wing where the shear layer was drawn into the main vortex system. At t=1.40, the main vortex structure is well established above the swept wing just aft of the mid-chord and is now much closer to the surface. The subsequent development of this vortex structure was unclear due to the diffusion of the smoke tracer in the region of interest.

In Fig. 10., at 73% of span, there is very little evidence of a dynamic stall vortex other than a small protuberance close to the leading edge at t=0.84. The free shear layer can be identified as a collection of smoke extending to the trailing edge downstream from just behind this disturbance. This appears to coalesce into a shear layer vortex which subsequently convects towards and off of the trailing edge. Possibly of more interest, however, is the strongly arched appearance of the flow over the front portion of the wing at t=1.0 and t=1.24. This is indicative of strong downwash from the tip vortex system affecting the aft portion of the chord.

Figure 11 shows the extent of the tip vortex system as viewed at the 90% of span location. In this case, separation appears to occur near the leading edge and the flow bears some resemblance to that which may be expected on a delta wing, albeit the vortex structure is not as compact.

By viewing the model from above and in front in Fig. 12., the full extent of the three dimensional effects across the span becomes apparent. At t=0.76, the dynamic stall vortex can be identified as a dense area of smoke at the mid-span and fainter bands of smoke on either side where the vortex is less well developed. Further outboard, in the swept area of the wing, there is no evidence of this vortex and the flow field appears to be dominated by the developing tip vortices.

At t=0.96, mid-span buckling of the dynamic stall vortex occurs in a similar manner to the behaviour observed on the straight wing. In this case, however, the distortion is much more concentrated in the mid-span region. Indeed, in subsequent frames, the dynamic stall vortex continues to rise from the surface but becomes more intense and contained within the mid-span region even although spatial continuity is apparently maintained with the outboard vortex sections. Meanwhile, the tip vortices appear to be increasing in strength and influencing a larger area of the span. This process continues until, at t=1.24, it is clear that the dynamic stall vortex is now highly arched and concentrated near the mid span. It is interesting to note that very little rearwards convection of the vortex system has taken place during this sequence of events.

From t=1.28 onwards, the mid-span segments of the dynamic stall vortex move slightly closer to the wing surface and the smoke in this region becomes more diffuse. As this happens, the spanwise extent of the vortex increases slightly, possibly indicating a reduction in the strength of the tip vortices. Indeed, at t=1.4, the smoke appears to be concentrated in two areas on either side of the mid-span . In this image, as with all the others in this sequence, there is clear evidence of connectivity between the dynamic stall vortex system and the tip vortices.

In the remaining frames of Fig. 12, the tip vortices continue to weaken and the smoke dissipates to leave a near uniform flow field at t=1.56.

The final set of images, presented in Fig. 13, show the wing as viewed from above and behind. At t=0.8, the tip vortices are well defined, dominating the swept areas of the planform and the dynamic stall vortex can be identified as a faint band of smoke upstream of the mid-chord region. A similar collection of smoke close to the trailing edge probably corresponds to the shear layer vortex. From t=0.88 onwards, two areas of smoke close to the mid-span are clearly defined and correspond to the formation of counter-rotating vortices at about 57% of span. As these vortices convect towards the mid-chord region, they move inwards and begin to elongate. At t=1.08, they are clearly elliptical and concentrated at the mid-span. Also in this frame, the tip vortices now engulf a larger area of the span and, although not obvious in this image, may have established contact with the outboard sections of the dynamic stall vortex at about 40% of chord.

As the area of smoke indicative of the counter-rotating vortices approaches the trailing edge it also begins to spread outwards, becoming more diffuse. Simultaneously, the weakening of the tip vortices is evidenced as they apparently move outboard and become barely distinguishable by t=1.56. In contrast to the behaviour observed from above and behind on the straight wing, the counter-rotating vortices here do not show any sign of convecting off the trailing edge as distinct coherent structures.

DISCUSSION

Rectangular planform

The results of the present flow visualisation study provide qualitative data on the unsteady flow field generated by the pitching motion of two different finite wing planforms. From this data, it is possible to begin to examine the complex vortical interactions which dominate three-dimensional dynamic stall. In this respect, this study will aid the interpretation of unsteady surface pressure data, recorded in the University of Glasgow's low speed 'Handley-Page' wind tunnel on identical wing planforms. Although, in this case, the flow visualisation tests were conducted at a different Reynolds number and reduced pitch rate from the other study, it may be expected that the gross flow features should be common to both sets of results.

Results presented in the previous section indicate that the unsteady flow field is dominated by two main vortical structures; the dynamic stall vortex emanating from the leading edge region and the tip vortices. A third structure, termed the shear layer vortex, which is a collection of vorticity originating in flow reversal near the trailing edge is also apparent in the flow field images. This structure, however, appears to have little influence on the main three-dimensional flow features. Nevertheless, the manner in which all three of these vortices influence and interact with one another yields a complex network of connectivity.

In steady flow, the spanwise loading distribution on a finite wing is dominated by the downwash from the wing tip vortices which becomes more significant nearer the wing tips and acts to reduce the effective incidence there. This effect produces spanwise pressure gradients which, together with the associated boundary-layer behaviour, contribute to a strongly three-dimensional flow field. Nevertheless, in the mid-span region, the flow on a wing of aspect ratio 3.0 would be expected to exhibit nominally two-dimensional characteristics.

The extension of this behaviour to the pitching wing would have two direct consequences. Firstly, flow patterns measured near the mid-span would correspond to previous visualisation studies of nominally two dimensional flow. This was indeed the case for the pitching rectangular wing where the images shown in Fig. 3 exhibit many of the classical features observed in studies on two-dimensional profiles at low Reynolds numbers. Subtle differences were apparent, however, particularly with respect to the height of dynamic stall vortex above the wing.

The second implication of extending the steady flow model relates to the resulting variation of effective pitch rate along the span. For the nominally two-dimensional case, it is generally accepted that the severity of the dynamic stall process is closely related to pitch rate, with high pitch rates producing the most severe dynamic loadings. Additionally, the triggering of dynamic stall events, in relation to the angle of attack, has also been found to be sensitive to the pitch rate with the dynamic stall vortex forming at higher angles with increasing pitch rate.

In the present study, the dynamic stall vortex was observed to initially form almost uniformly along the span. This is, in fact, consistent with the expected behaviour since the effective incidence will vary along the span as will the effective pitch rate. Very quickly, however, the apparent two dimensionality of the vortex is replaced by a strongly three dimensional system. Once again this could be anticipated as the segments of the vortex near the mid-span, where the effective pitch rate is highest and the rate or change of pressure gradient is most severe, would be expected to experience a more rapid increase in strength. The resulting effect is to produce a strong inboard spiralling along the vortex to feed the mid-span region.

Chordwise convection of the dynamic stall vortex occurs almost immediately in the mid-span region. Conversely, on outboard sections, no significant evidence of vortex convection exists. This behaviour, together with non-uniform elevation of the vortex from the wing surface, results in a complex three-dimensional vortex system. The mechanism which produces this effect appears to be a result of the basic three-dimensional characteristics already described. In particular, the flow along the vortex towards the mid-span region inevitably accelerates the vortex growth there. This growth is further enhanced by the entrainment of the mid-span segments of the shear-layer vortex into the dynamic stall vortex. The resulting effect is to lift the vortex core from the surface more rapidly than in a nominally-two dimensional flow where there is no spanwise inflow to the vortex. On outboard sections, vortex growth is retarded by the downwash from the wing tips and the same effect acts to pull the vortex down towards the surface.

The inevitable outcome of the two conflicting effects at the mid-span and the tips is the buckling of the dynamic stall vortex, as observed in Fig. 7. Through the necessity to retain vortex connectivity, weak outboard segments of the stall vortex are linked to the strong mid-span segment by the tornado-like spirals apparent in Fig. 4. at the 73% of span location. These linking segments, when viewed from above in Fig. 6, appear as concentrated areas of counter-rotating smoke but are, as indicated, part of a connected vortex system. As this system develops, the mid-span portion is apparently held near the mid-chord whilst it amalgamates with the remainder of the mid sections of the shear layer vortex. At this point, the two counter-rotating spirals begin to draw fluid inwards from the outboard sections of the shear layer vortex, thus establishing a connectivity path to the wing tip trailing edges and the tip vortex.

While the main sections of the vortex system are held near the mid-chord, the outboard segments appear to significantly dissipate. There is no noticeable convection of these sections but the central portion convects rearwards and the two counter-rotating segments become more inclined to the mean flow direction. Thus, as may be observed in Figs. 3 and 6, the counter-rotating spirals are still visible on the wing after the centre portion of the vortex has left the trailing edge. Subsequently, these features also convect towards the trailing edge moving closer to each other as they do. This is probably due to the constriction of the flow on the rear of and behind the wing created by the trailing tip vortices, as observed by Freymuth[5]. Finally, the twin spirals convect off the trailing edge and the wing reverts to the true bluff body state.

Swept-tip planform

The unsteady flow field which evolves over the swept wing appears to be governed by the same three vortical structures which were observed on the straight wing. There are, however, some significant differences in the manner in which these systems interact. On the swept-tip wing, the tip vortices are larger and their orientation is such that they directly influence a greater proportion

of the wing. This suggests that the effect of downwash across the swept wing should be more pronounced leading to lower effective reduced pitch rates along the span than on the previous model. One immediate consequence of this is that the dynamic stall vortex on the swept-tip wing will be weaker than its straight wing counterpart. Indeed, Fig. 8. the weakness of the vortex is clear when compared to the images from the straight wing at 52% of span. Regardless of this, it is pertinent to note that the vortex is still a major feature of the developing flow field.

Once again, many of the features observed on the rectangular planform were present on the swept-tip wing. In particular, an upward buckling of the dynamic stall vortex was observed at the mid-span in Fig 12. As in the previous case, the elevated section of the vortex appeared to maintain spatial continuity with the outboard sections through tornado-like spirals. In this case, however, the rise of the vortex at the mid span was initiated earlier and it did not amalgamate with the shear layer vortex. This is a consequence the inherently weak dynamic stall vortex resulting from the lower effective reduced pitch rate and is consistent with corresponding results from nominally two-dimensional flows [6].

Another important difference between the two flows is the spanwise distribution of the vortex structures. Care must be taken, however, when interpreting the results since, although the span of the two wings is the same, the effective aspect ratio of the swept-tip wing is only 2.42. Thus, it would be reasonable to expect some concentration of flow features in this case. Nevertheless, the obvious strength of the wing tip vortices plays a pivotal role in the flow field structure, resulting in even greater inboard compression of flow features than a simple allowance for aspect ratio would warrant. Consequently, when viewed from above and behind in Fig. 13, the counter-rotating vortices, which connect the central vortex segment to the outboard sections, are evident at 57% of span as opposed to 73% for the straight wing. Subsequently, as they convect aft, they move inwards towards each other and appear to elongate. This behaviour may be due to a combination of the mutual attraction between these vortices and the physical constriction imposed by the tip vortices.

Subsequent development of the elevated mid-span portion of the dynamic stall vortex is strongly affected by the change in tip geometry. Side view pictures at 52% of span in Fig. 8 indicate that once the vortex has lifted away from the surface it tends to remain above the mid-chord region. This behaviour is quite different to the straight wing case where, although the downstream progression of the vortex is momentarily delayed near the mid-chord, it continues to convect downstream and off the trailing edge. In Fig. 8. the vortex above the swept wing appears to elongate at t=1.2 as it resists the freestream influence. The reason for this deformation is not clear, although pictures from the front in Fig. 12 suggest that it may be due to the attractive force created by the inboard sweep of the tip vortex systems. Subsequently, the dynamic stall vortex can be observed to break up over the wing.

CONCLUSIONS

At the reduced pitch rate considered in this study, the dynamic stalling of a finite rectangular wing of aspect ratio 3 was found to be dominated by the tip and dynamic stall vortex systems.

The initial development of stall was found to be almost uniform along the span. Subsequent development of the flow during stall was strongly three-dimensional although many of the classical features of nominally two-dimensional flow were present near the mid-span.

The development of stall on the swept-tip wing was dominated by the same flow structures as were present on the rectangular planform. The relative strengths of the two vortex systems were, however, quite different, resulting in significant differences in the nature of stall.

ACKNOWLEDGEMENTS

The authors wish to acknowledge the assistance provided by Prof. R.A.McD. Galbraith and Dr. R. Green of the Department of Aerospace Engineering, Glasgow University. The authors also wish to acknowledge the financial support of the Nuffield Foundation Undergraduate Research Bursary programme (NUF-URB95).

REFERENCES

1. Carr, L., 'Progress in the analysis and prediction of dynamic stall', Journal of Aircraft, Vol. 25, No. 1, 1988

2. Peziali, R.A . '2-D and 3-D Oscillating Wing Aerodynamics for a Range of Angles of Attack Including Stall.', NASA-TM-4632, 1994

3. Horner, M.B., Addington, G.A., Young III, J.W., Luttges, M.W., 'Controlled Three-Dimensionality in Unsteady Separation Flows about a Sinusoidally Oscillating Flat Plate.', AIAA- 90-0689, 1990

4. Galbraith, R.A.McD., Coton, F.N., Jiang, D. and Gilmour, R. 'Preliminary results from a three-dimensional dynamic stall experiment of a finite wing', presented at 21st European Rotorcraft Forum, St. Petersburg, Russia, 1995, Paper II-3.

5. Freymuth, P., 'Visualising the connectivity of vortex systems for pitching wings', Journal of Fluids Engineering, Vol. 111, 1989

6. McCroskey, W.J., 'The phenomenon of dynamic stall', NASA TM-81264, 1981

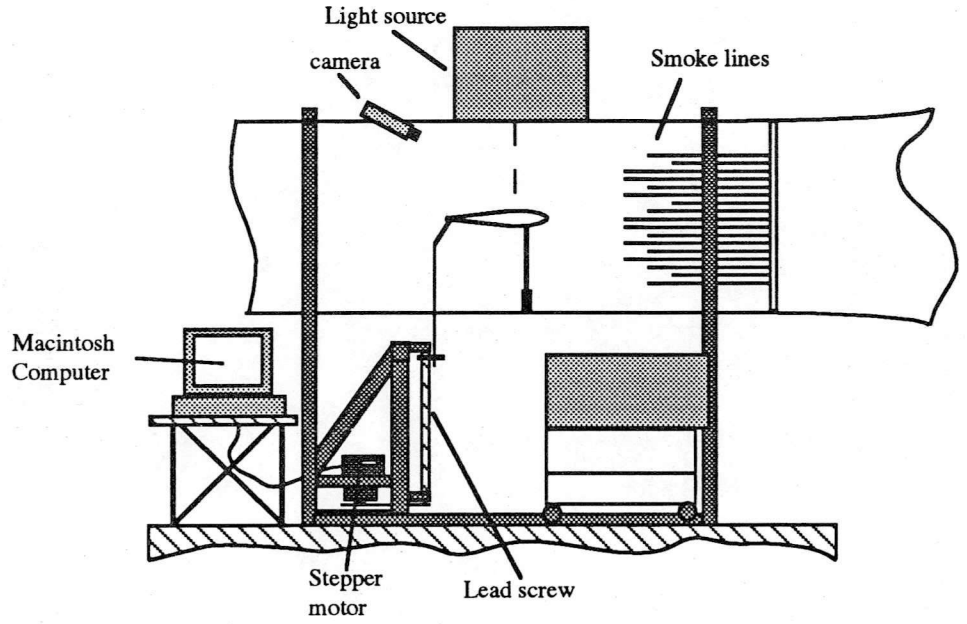

Fig. 1. Test set-up

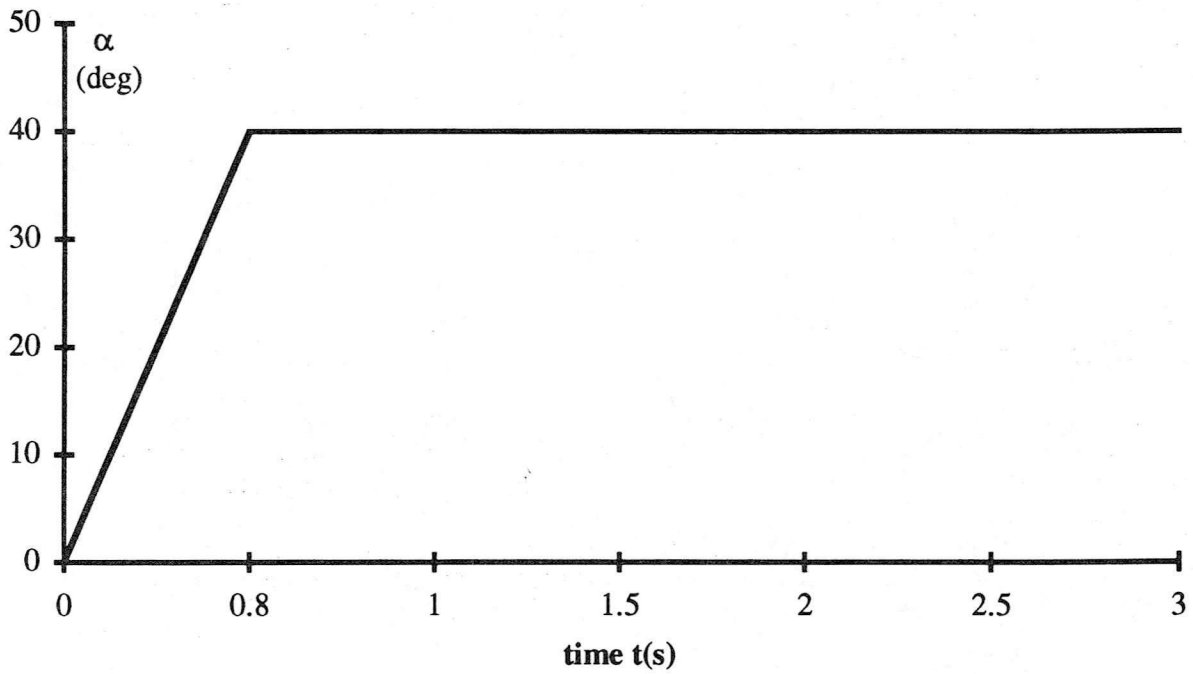

Fig. 2. Incidence variation against time

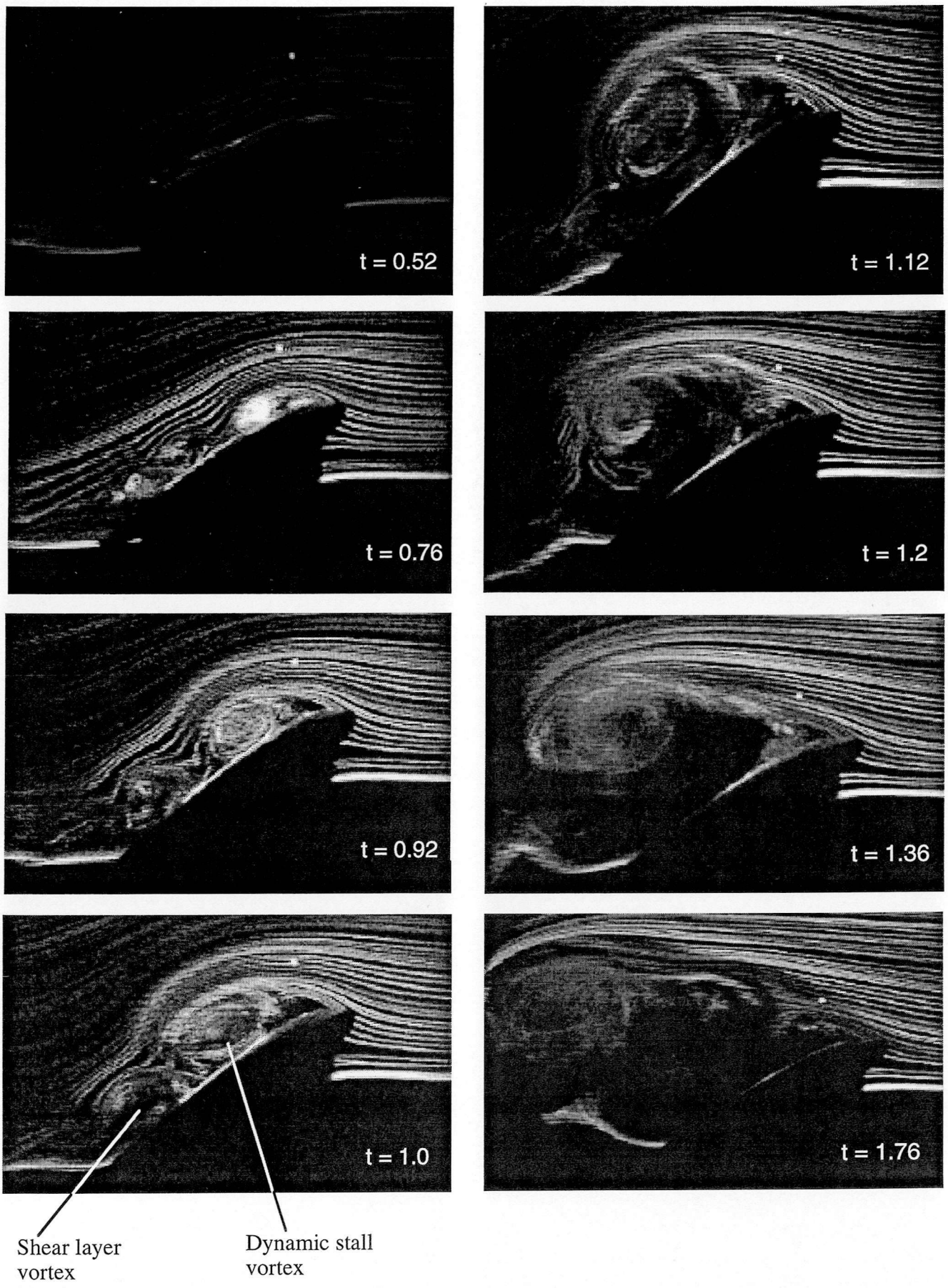

Fig. 3. Images recorded at 57% of span of rectangluar wing

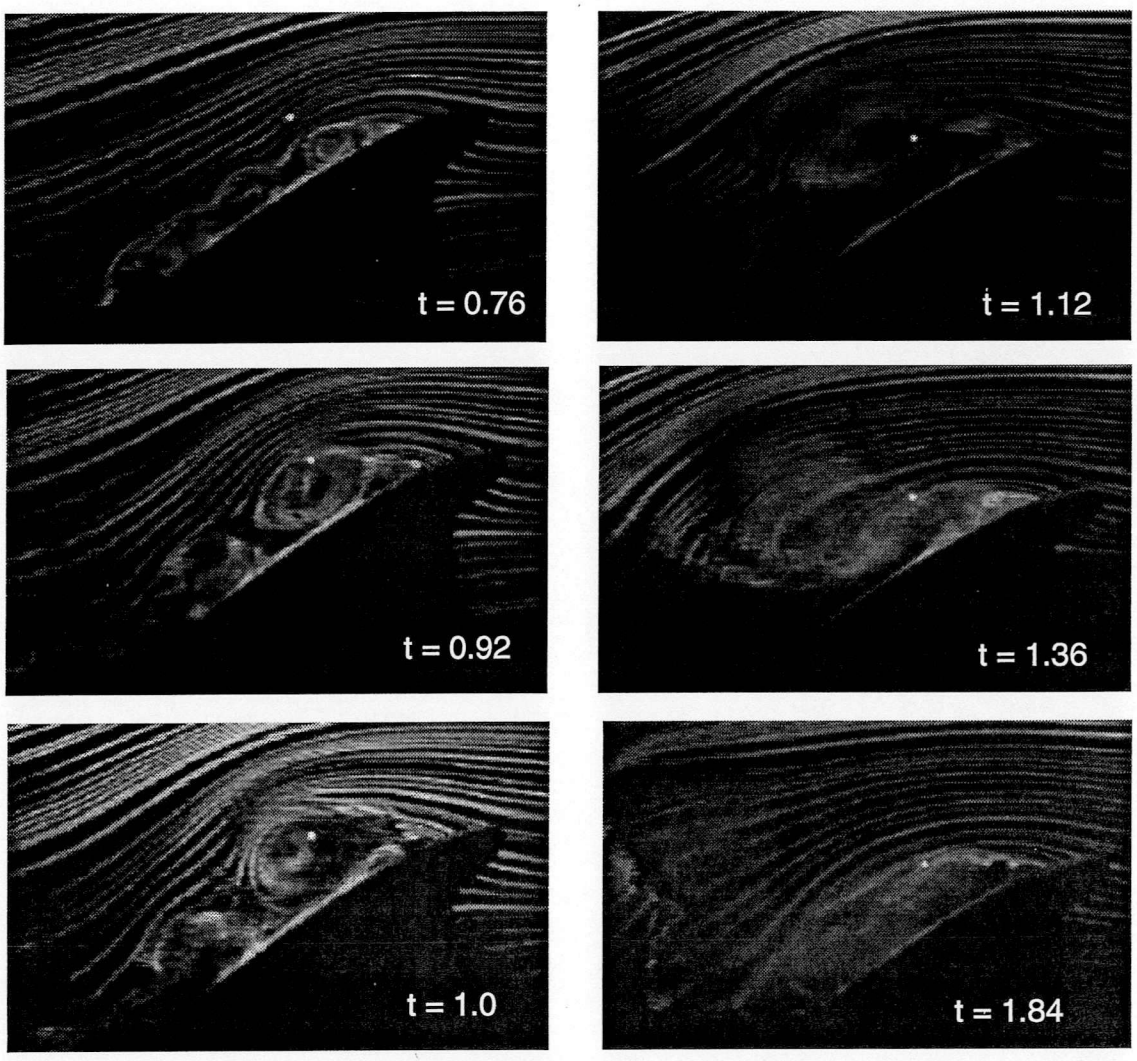

Fig. 4. Images recorded at 73% of span of rectangluar wing

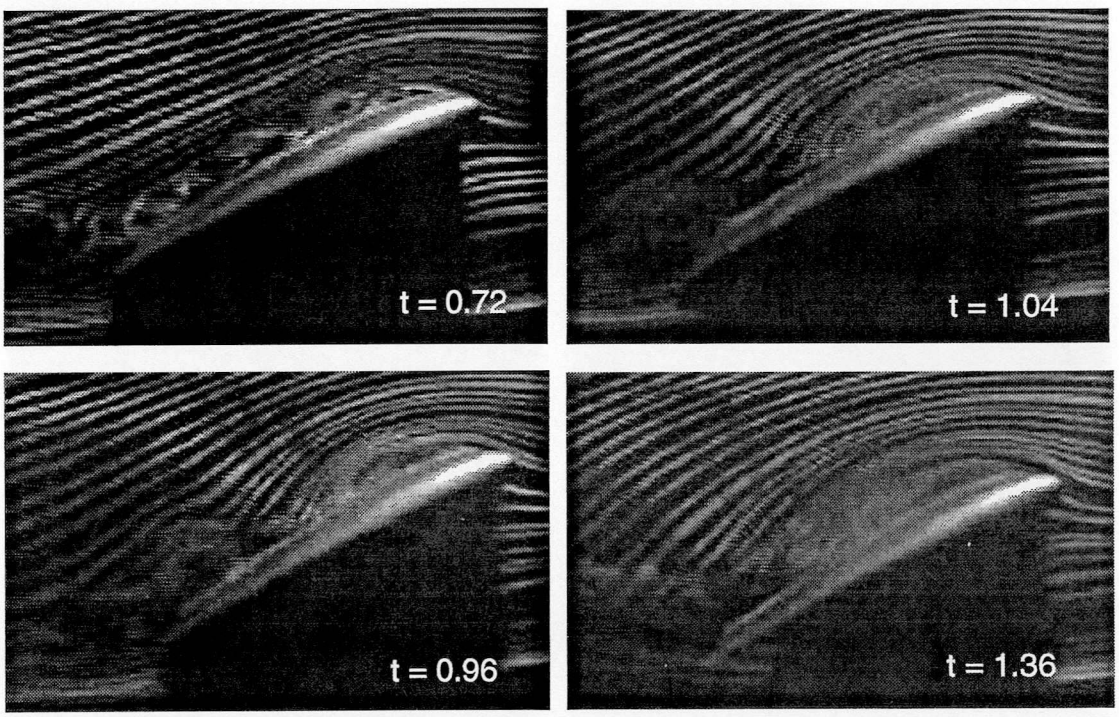

Fig. 5. Images recorded at 90% of span of rectangluar wing

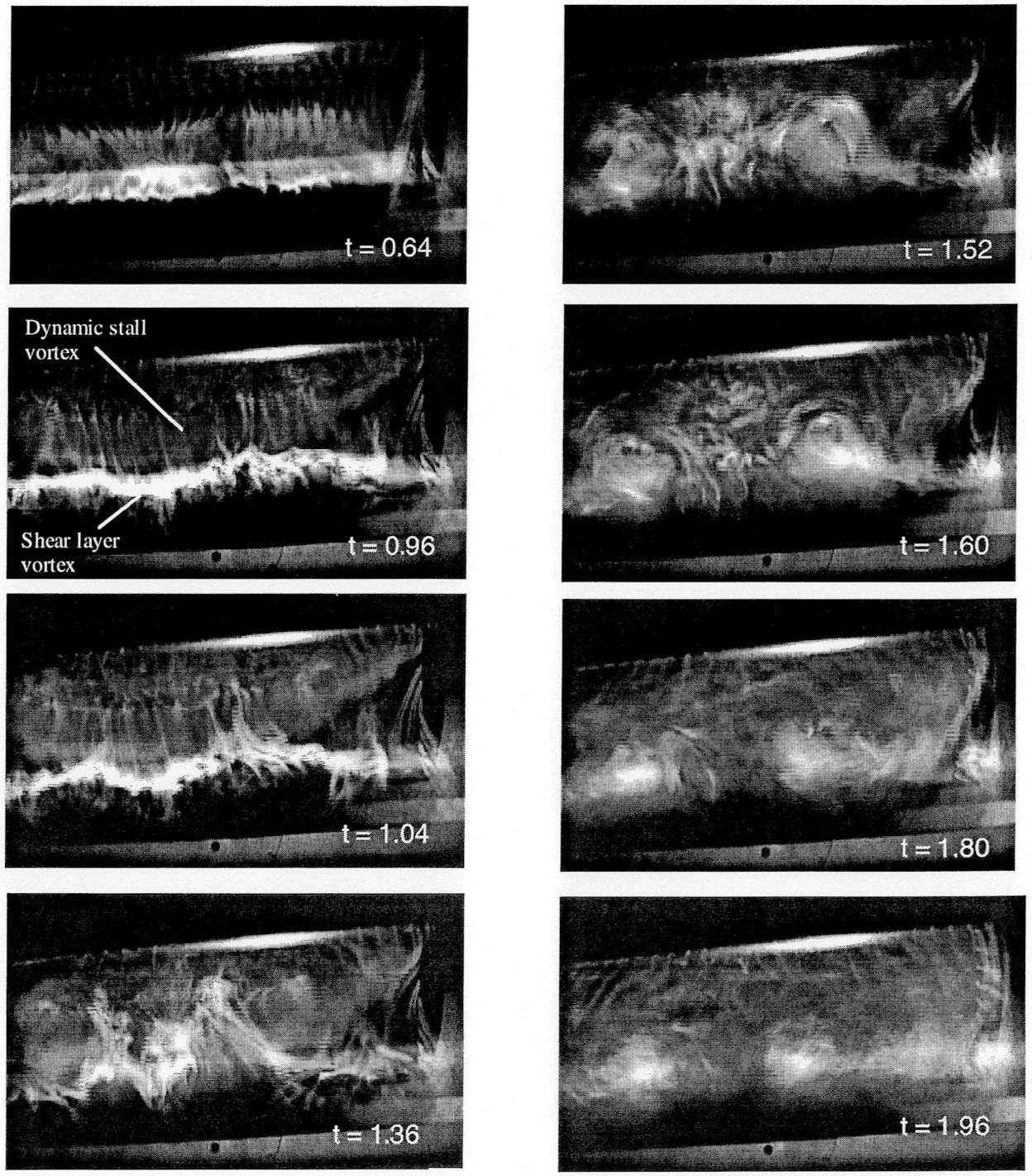

Fig. 6. View of rectangular wing from above and behind

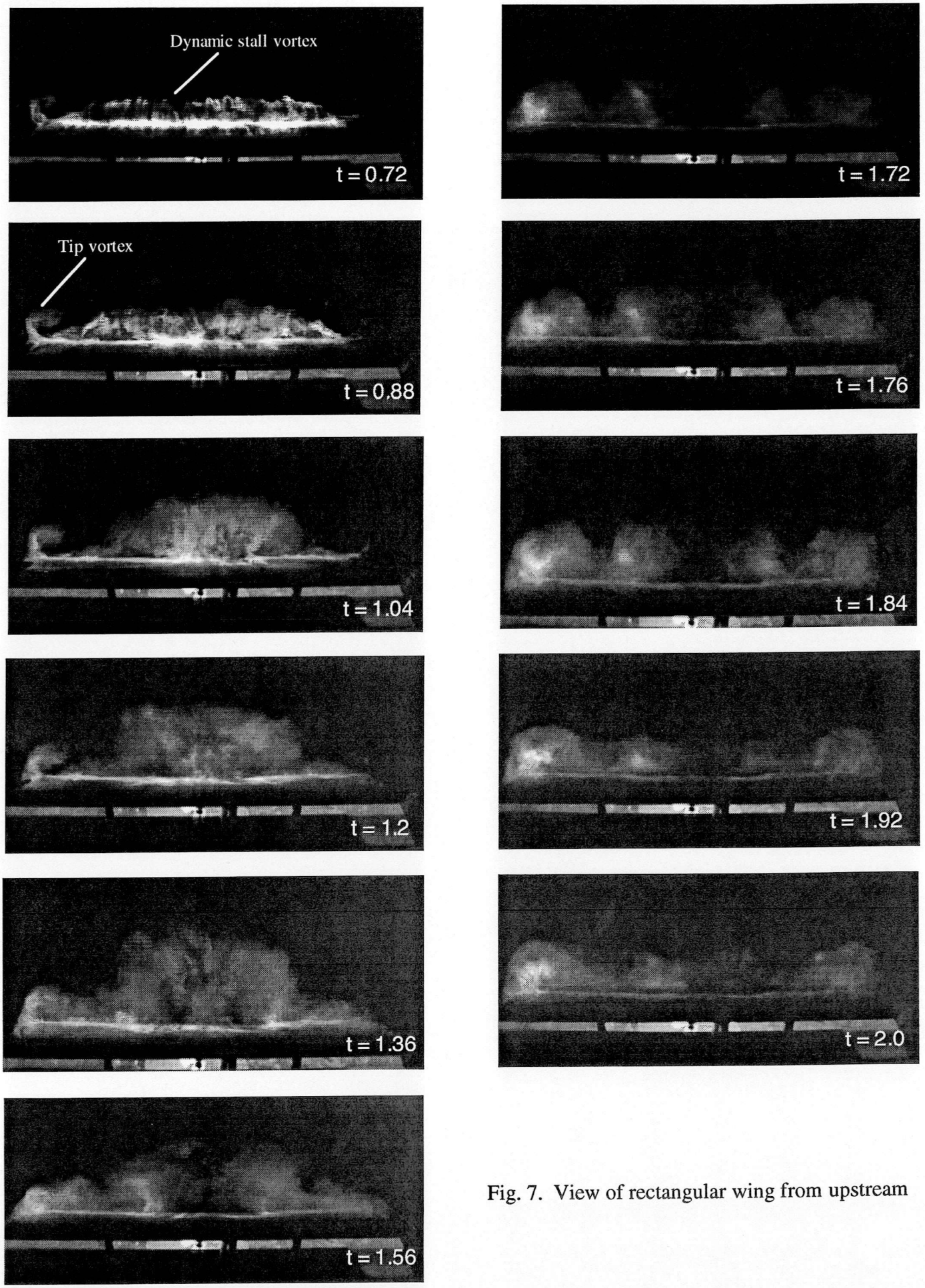

Fig. 7. View of rectangular wing from upstream

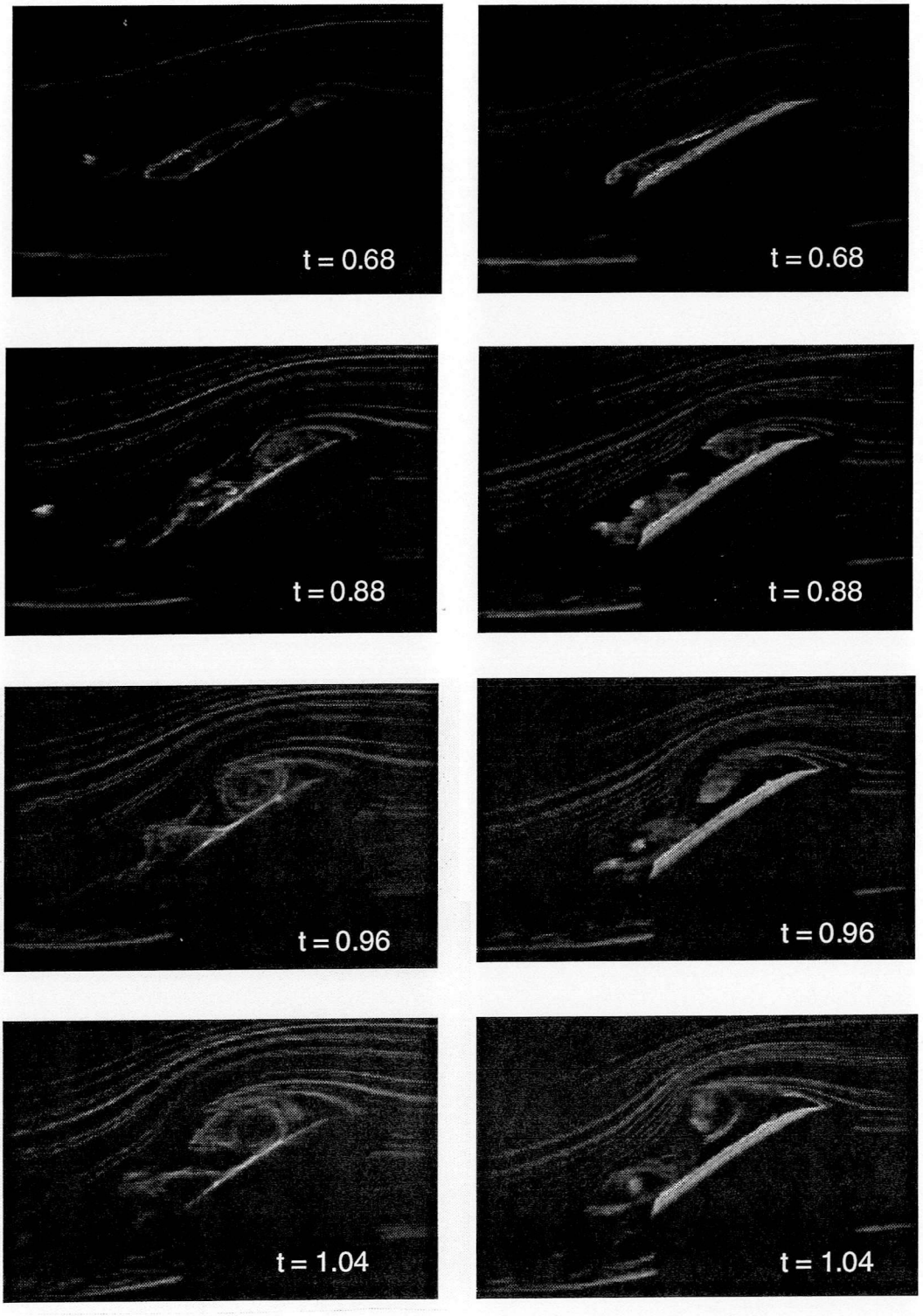

Fig. 8. Comparison of images from rectangular wing and rectangular wing with swept tips at 52% of span

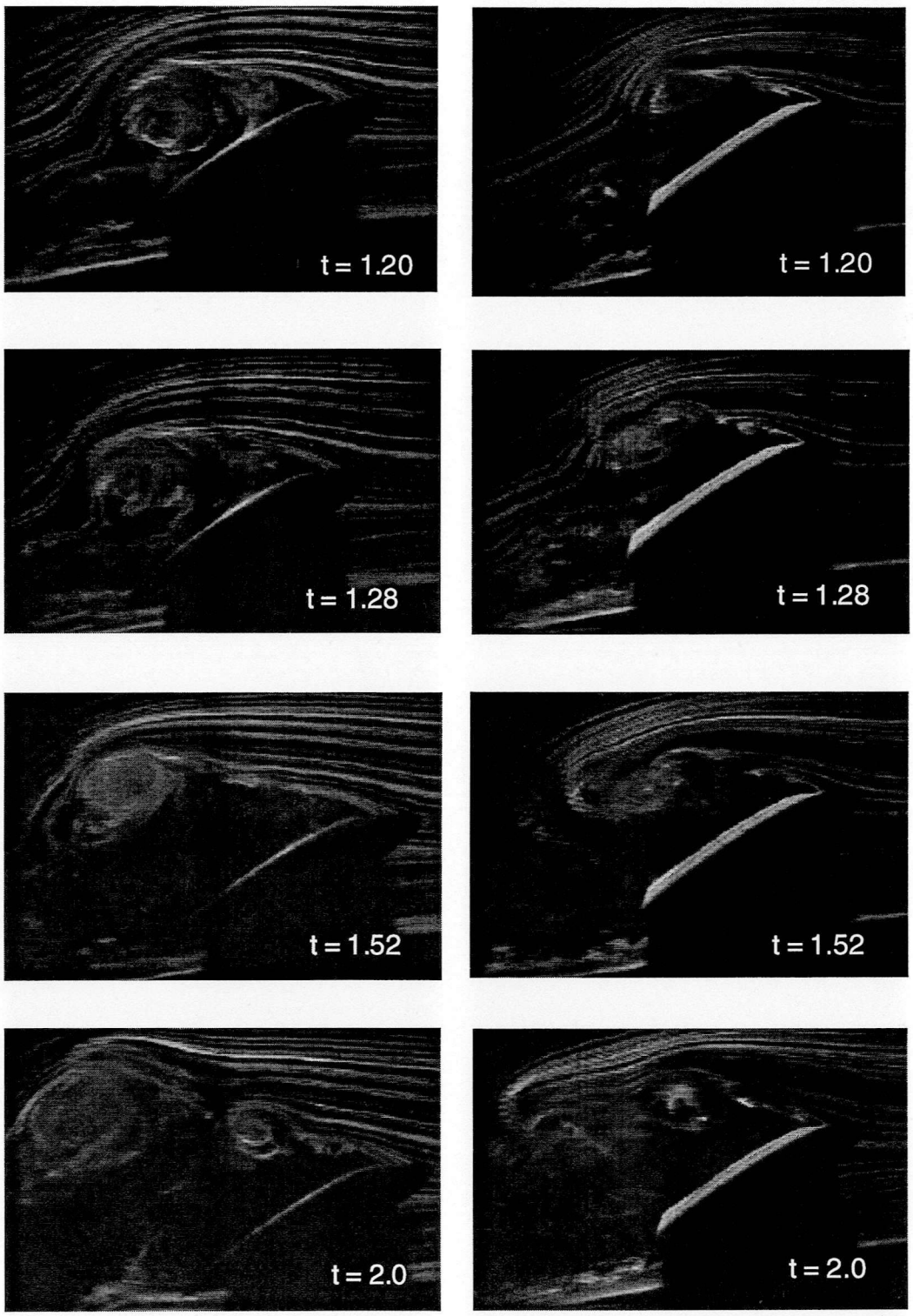

Fig. 8. (Continued)

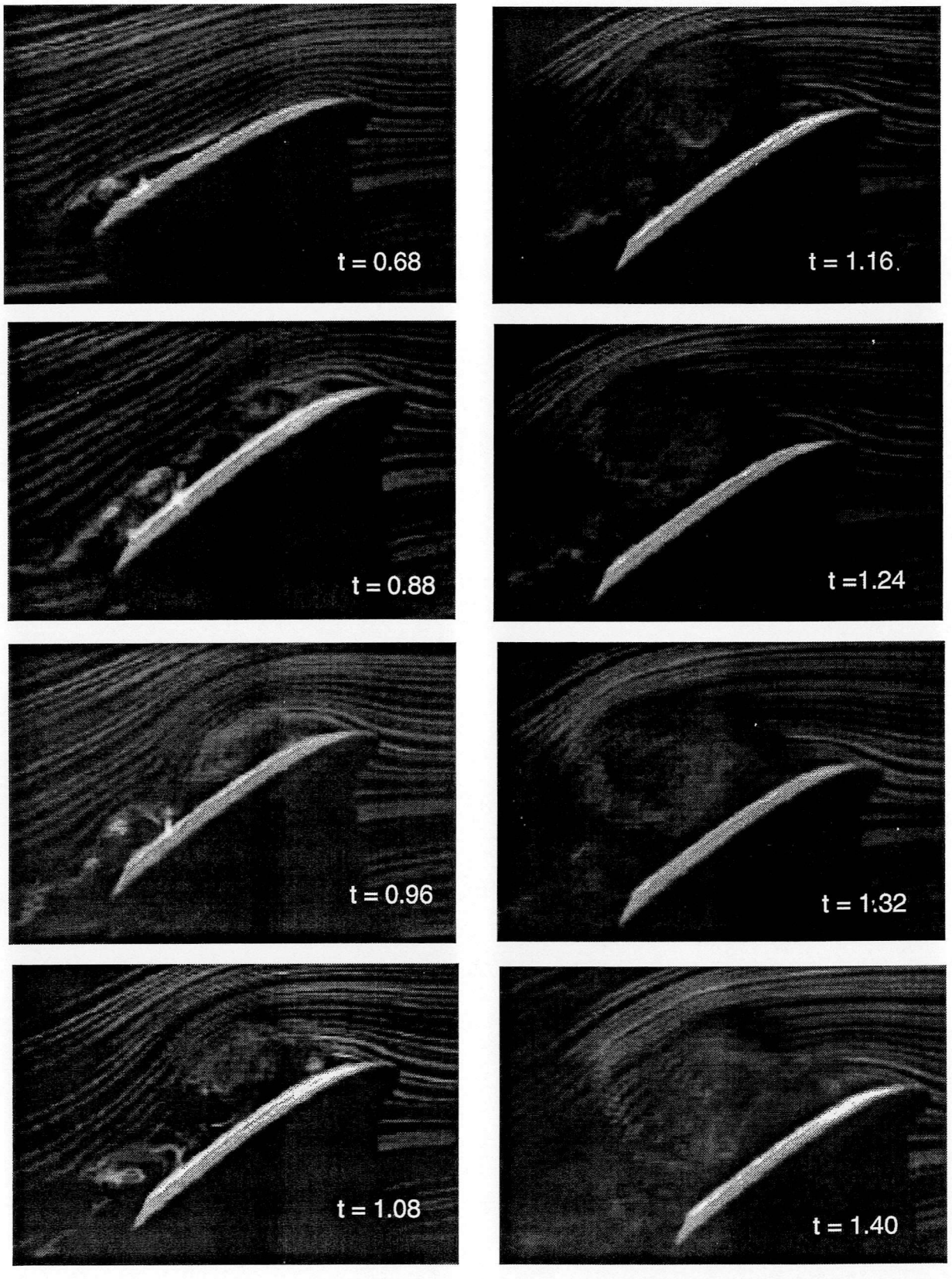

Fig. 9. Images recorded at 57% of span of rectangluar wing with swept tips

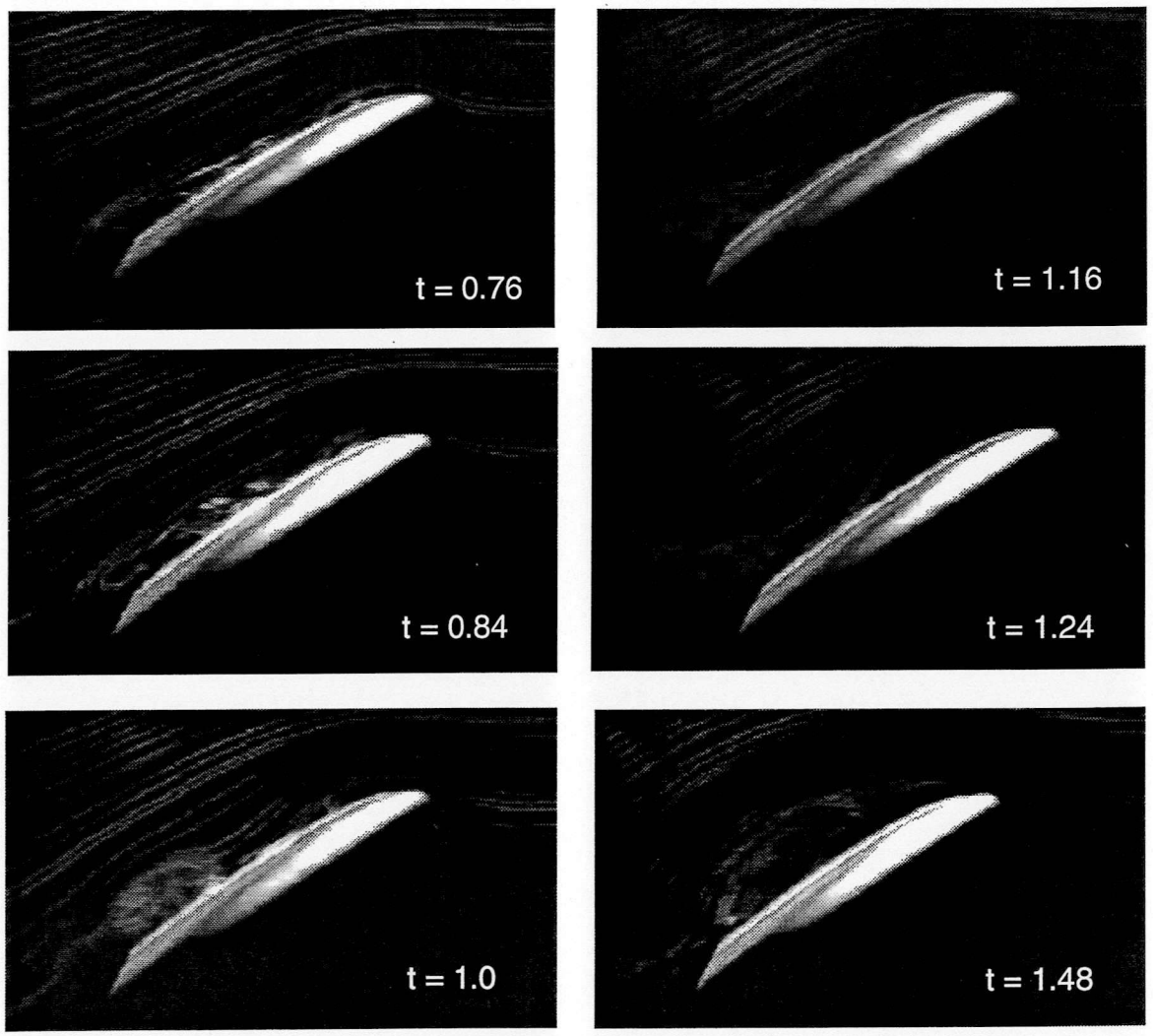

Fig. 10. Images recorded at 73% of span of rectangluar wing with swept tips

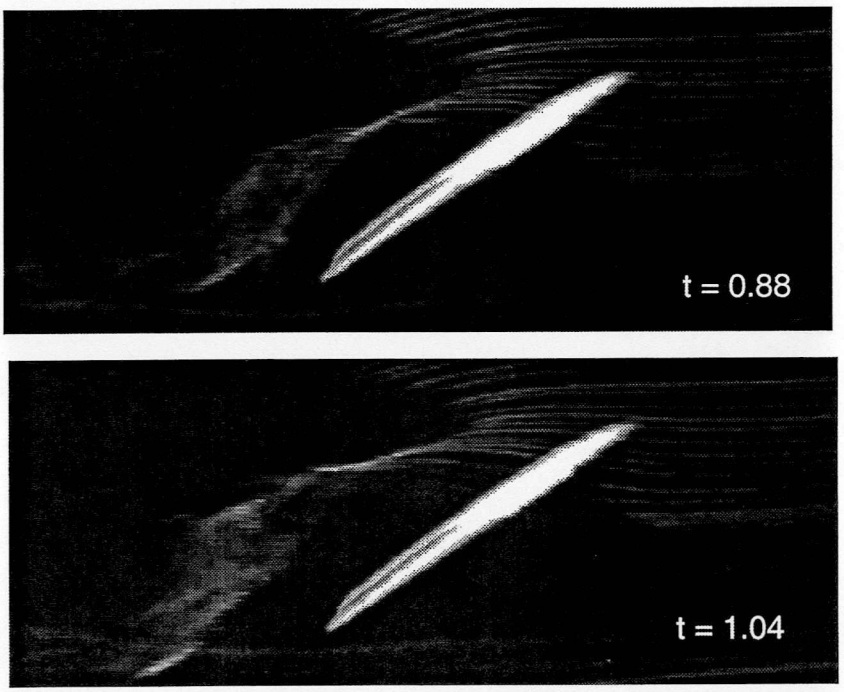

Fig. 11. Images recorded at 90% of span of rectangluar wing with swept tips

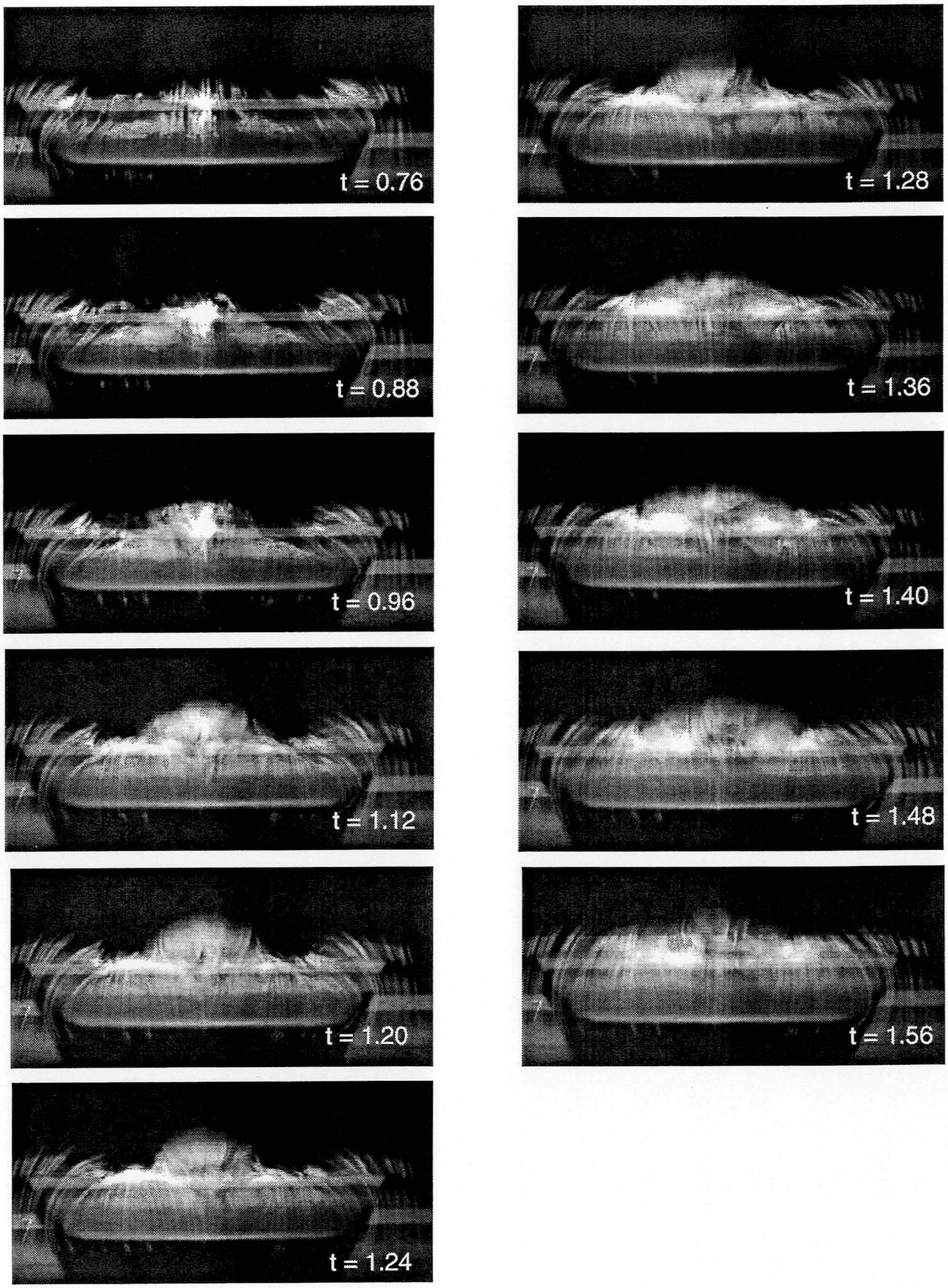

Fig. 12. View of rectangular/swept wing from upstream

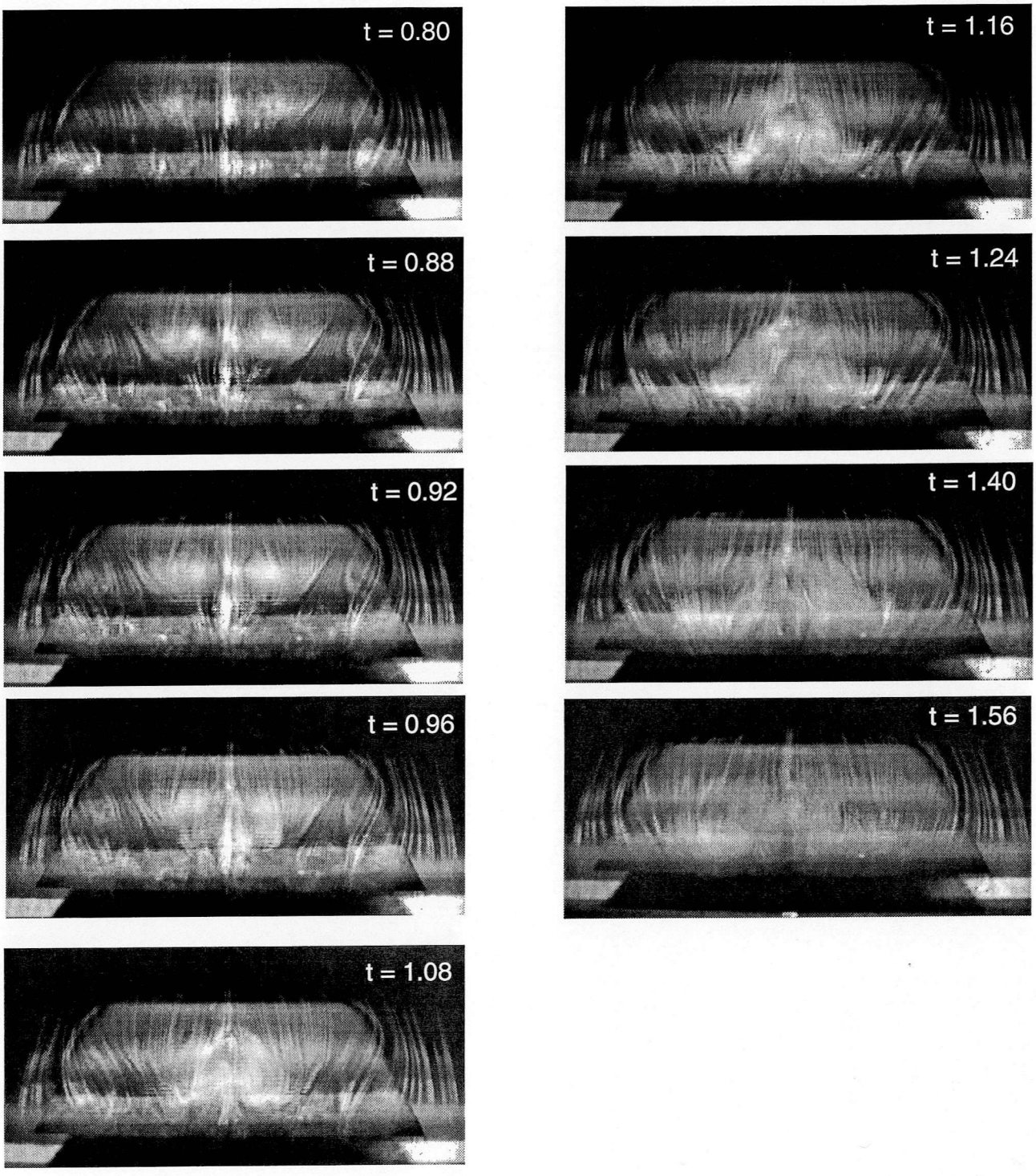

Fig. 13. View of rectangular/swept wing from above and behind